

Non-local Coulomb interactions and metal-insulator transition in Ti_2O_3 : a cluster LDA+DMFT approach.

A.I. Poteryaev,¹ A.I. Lichtenstein,¹ and G. Kotliar²

¹*ESM, University of Nijmegen, NL-6525 ED Nijmegen, The Netherlands*

²*Serin Physics Laboratory, Rutgers University, Piscataway, New Jersey 08855*

(Dated: November 16, 2018)

We present an *ab initio* quantum theory of the metal-insulator transition in Ti_2O_3 . The recently developed cluster LDA+DMFT scheme is applied to describe the many-body features of this compound. The conventional single site DMFT cannot reproduce a low temperature insulating phase for any reasonable values of the Coulomb interaction. We show that the non-local Coulomb interactions and the strong chemical bonding within Ti-Ti pair is the origin of the small gap insulating ground state of Ti_2O_3 .

PACS numbers: 71.15.-m, 71.27.+a, 71.30.+h

The complicated electronic structure and the nature of the metal-insulator transition in Ti_2O_3 and V_2O_3 has been the object of intensive experimental and theoretical investigation over the past half century [1]. Recent progress in high-energy photo-emission spectroscopy [2] and correlated electrons dynamical-mean field theory (DMFT) [3] has shed new light on the first-order metal-insulator transition in V_2O_3 . It has been shown that an realistic description of the metallic and insulating phases of V_2O_3 can be obtained from the combination of a band structure scheme with the local electron-electron interaction given from DMFT [4]. The correlation effects in Ti_2O_3 are less clear but angle resolved photo-emission experiment [5] shows a strong reduction of the Ti $3d$ -bandwidth compared to band structure calculations. The important question is related to the mechanism of the small, about 0.1 eV, semiconductor band-gap formation. The generally accepted view is that the metal-insulator transition is related to the decrease of the c/a ratio in rhombohedral Ti_2O_3 and the formation of a Ti-Ti pair along z -axis [6]. Below the broad (almost 250 K in width) metal-insulator transition at around 470 K the Ti-Ti pair distance is seen to decrease without any change of the rhombohedral structure or the formation of long-range antiferromagnetic order [7]. This is in contrast to the case of V_2O_3 where the V-V pair distance increases within a monoclinic distortion in the antiferromagnetic phase [1].

Ti_2O_3 has an $\alpha\text{-Al}_2\text{O}_3$ corundum structure (Fig. 1) in the metallic and insulating phases with two formula units per rhombohedral cell [8]. Each Ti atom is surrounded by the octahedron of oxygens leading to the large $t_{2g}\text{-}e_g^\sigma$ splitting. The trigonal distortion gives an additional splitting of t_{2g} bands into $e_g^\pi\text{-}a_{1g}$ states and a_{1g} subbands of Ti-Ti pair form strong bonding-antibonding counterparts (Fig. 1). In principle, the large decrease of the Ti-Ti distance could split further an occupied single-degenerate a_{1g} states from a double-degenerate e_g^π states of t_{2g} subband and form the insulating d^1 configuration of this Ti compound. Nevertheless, state of the art LDA calculations have shown that for reasonable Ti-Ti pair

distances Ti_2O_3 will stay metallic [9].

In order to investigate the role of electron-electron interactions in the formation of this insulating low-temperature phase one needs an accurate estimation of the a_{1g} and e_g bandwidths in this complex structure [10]. For example a simple free $[\text{Ti}_2\text{O}_9]^{12-}$ cluster mean-field investigation can easily produce a semiconducting gap due to drastic underestimation of the a_{1g} and e_g bandwidths [11]. On the other hand a more accurate band structure calculation within the unrestricted Hartree-Fock approximation results in large gap antiferromagnetic state [12]. Thus it is crucial to use both the correct Green-function embedding of the Ti-Ti pairs as well as a more accurate treatment of the electron-electron interaction.

The role of metal-metal pair formation and the "molecular" versus band pictures of the electronic structure have attracted much attention in these compounds [13]. The combination of a strong on-site Coulomb interaction and the large anisotropy between the hopping parameters in and perpendicular to the pair direction can favor a localized molecular-orbital picture of the insulating phase. However, realistic tight-binding calculations for V_2O_3 have shown the importance of long-range hopping parameters [14]. It is also unclear how good an on-site approximation is for the electron-electron interaction. Since the pair forms a natural "molecular like" element in the corundum-type Ti_2O_3 structure it might be expected that non-local electron correlations are important in this system. Thus an approach which combines pair and beyond pair hopping with non-local electron interactions would be seem to be ideal for this problem.

In this letter we apply for the first time a method, the cluster DMFT scheme [15, 16], which contains all the physics of correlated pairs in crystals to determine the origin of the insulating phase and the metal-insulator transition in Ti_2O_3 . A numerically exact multi-orbital Quantum Monte-Carlo (QMC) scheme is deployed for the solution of the cluster DMFT problem and an accurate first principles tight-binding parametrization used for the

one electronic structure. Our strategy here is to investigate the gap formation using single site [17] and cluster LDA+DMFT with only local correlations included. We then deploy the full non-local CDMFT and in this way are able to directly elucidate the impact non-local Coulomb interactions have on the physics. We show that the competition between strong bonding within the Ti-Ti pair and localization from correlation effects leads to the unique situation of the small semiconducting gap structure in Ti_2O_3 oxide and that non-local Coulomb correlations are of crucial importance for the physics of this small gap insulators.

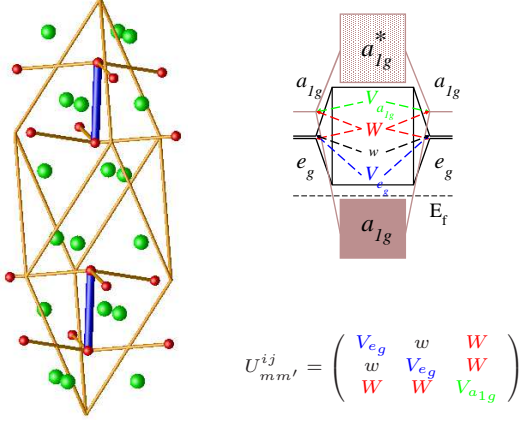


FIG. 1: Left - rhombohedral unit cell of Ti_2O_3 corundum structure. Titanium ions are indicated by the red color, oxygens by green, and the pair of Ti atoms in z direction by blue. Right - schematic representation of the t_{2g} splitting in Ti_2O_3 (top part) and the intersite Coulomb interaction matrix (bottom part). $w=0$ in all our calculations.

We start with the orthogonal LDA Hamiltonian $H_{mm'}^{LDA}(\mathbf{k})$ in the massively downfolded N-th order muffin-tin orbital representation [18] (m corresponds to the 12 t_{2g} orbitals of two Ti-Ti pairs in rhombohedral unit cell) and include different Coulomb interactions (see Fig. 1). DMFT results for the local and non-local Coulomb interactions are presented in Figs. 2,3.

The bare LDA density of states (DOS) is shown in Fig. 3 by the dashed lines for the low temperature structure (LTS, ~ 300 K [8]) and high temperature structural (HTS, ~ 870 K [8]) data on the upper and lower panels respectively. Both LTS and HTS electronic structures are metallic within the LDA scheme. The a_{1g} subband (green dashed line in the Fig. 3) has a strong bonding-antibonding splitting in contrast to the e_g^π subbands (red dashed line). The bandwidth of the HTS is approximately 2.8 eV and smaller than the bandwidth of the LTS (3.2 eV) due to the reduction of the $t_{a_{1g}, a_{1g}}$ hopping from -0.85 to -0.63 eV.

The cluster DMFT maps the many-body crystal system onto an effective self-consistent multi-orbital quantum impurity-cluster problem [15, 16]. The corresponding Green-function matrix for the Ti-Ti cluster in the

LDA+DMFT scheme is calculated via the BZ-integration

$$\mathbf{G}(i\omega_n) = \sum_{\mathbf{k}} [(i\omega_n + \mu)\mathbf{1} - \mathbf{H}^{LDA}(\mathbf{k}) - \mathbf{\Sigma}(\omega_n)]^{-1}, \quad (1)$$

where μ is the chemical potential defined self-consistently through the total number of electrons, $\omega_n = (2n + 1)\pi T$ are the Matsubara frequencies for temperature $T \equiv \beta^{-1}$ ($n = 0, \pm 1, \dots$) and σ is the spin index. The Hamiltonian and the self-energy matrix have the following supermatrix form corresponding to the symmetry of two Ti-Ti pairs in the unit cell

$$\begin{pmatrix} \mathbf{H}_{11} + \mathbf{\Sigma}_{11} & \mathbf{H}_{12} + \mathbf{\Sigma}_{12} & \mathbf{H}_{13} & \mathbf{H}_{14} \\ \mathbf{H}_{21} + \mathbf{\Sigma}_{21} & \mathbf{H}_{22} + \mathbf{\Sigma}_{11} & \mathbf{H}_{23} & \mathbf{H}_{24} \\ \mathbf{H}_{31} & \mathbf{H}_{32} & \mathbf{H}_{33} + \mathbf{\Sigma}_{11} & \mathbf{H}_{34} + \mathbf{\Sigma}_{12} \\ \mathbf{H}_{41} & \mathbf{H}_{42} & \mathbf{H}_{43} + \mathbf{\Sigma}_{21} & \mathbf{H}_{44} + \mathbf{\Sigma}_{11} \end{pmatrix}, \quad (2)$$

where $\mathbf{H}_{ij}(\mathbf{k})$ and $\mathbf{\Sigma}_{ij}(\omega_n)$ are 3×3 matrices for the t_{2g} states and $\mathbf{\Sigma}_{11}$ and $\mathbf{\Sigma}_{12}$ correspond to the intrasite and intersite contributions to the self-energy respectively.

In the self-consistent cluster DMFT scheme the local Green-function (1) should coincide with the corresponding solution of the effective two-site quantum impurity problem [3]

$$\mathbf{G}_\sigma(\tau - \tau') = -\frac{1}{Z} \int D[\mathbf{c}, \mathbf{c}^+] e^{-S_{eff}} \mathbf{c}(\tau) \mathbf{c}^+(\tau') \quad (3)$$

here $\mathbf{c}(\tau) = [c_{im\sigma}(\tau)]$ is the super-vector of the Grassman variables, Z is the partition function, i runs over Ti-Ti pair and m runs over e_g^π or a_{1g} orbitals. The effective cluster action S_{eff} is defined in terms of so-called ‘‘bath’’ Green function matrix [3] $\mathcal{G}_\sigma^{-1}(\omega_n) = \mathbf{G}_\sigma^{-1}(\omega_n) + \mathbf{\Sigma}_\sigma(\omega_n)$ which describes the energy, orbitals, spin and temperature dependent interactions of particular cluster with the rest of the crystal

$$S_{eff} = - \int_0^\beta d\tau \int_0^\beta d\tau' Tr[\mathbf{c}^+(\tau) \mathcal{G}^{-1}(\tau, \tau') \mathbf{c}(\tau')] + \frac{1}{2} \sum_{im, jm', \sigma} [U_{mm'}^{ij} n_{im}^\sigma n_{jm'}^{-\sigma} + (U_{mm'}^{ij} - J_{mm'}^{ij}) n_{im}^\sigma n_{jm'}^\sigma] \quad (4)$$

here $n_{im\sigma} = c_{im\sigma}^\dagger c_{im\sigma}$. We have parameterized the screened local Coulomb and exchange matrices ($U_{mm'}^{ii}$ and $J_{mm'}^{ii}$) for the t_{2g} electrons in terms of average Coulomb and exchange integrals [19] and used a simple approximation to the intersite $U_{mm'}^{ij}$ interactions as shown in the Fig. 1.

The multi-band impurity QMC scheme [20, 21] has been used for the numerically exact calculation of the cluster Green function (eq. 3). The number of auxiliary Ising fields in the discrete Hirsh-Fye transformation were 15 and 58 for the local and non-local Coulomb interaction schemes respectively. For accurate QMC integration we used of the order of 10^6 sweeps, with 8000 \mathbf{k} -points for the BZ-integration. Within 15-20 DMFT iterations

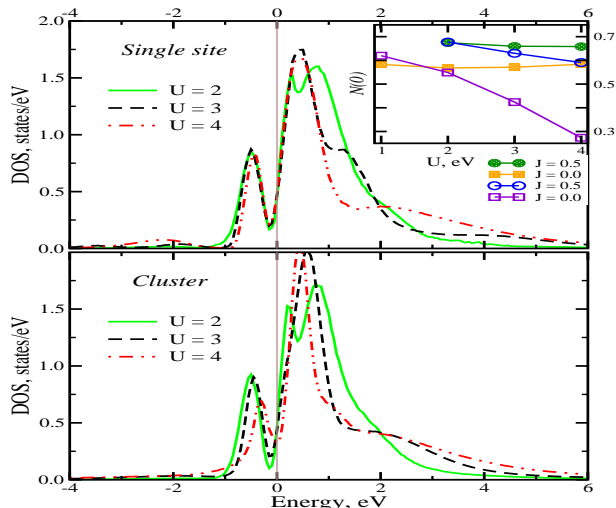


FIG. 2: Density of states for the single site (upper panel) and cluster (lower panel) DMFT calculations with different values of the Coulomb repulsion U and $J=0.5$ eV. Inset: $N(0)$ versus Coulomb parameter. Filled dark green circles - DMFT results with $J=0.5$ eV, filled orange squares - DMFT with $J=0$ eV. Open blue circles and violet squares are CDMFT with $J=0.5$ and 0 eV respectively.

convergence in the self-energy was reached. The maximum entropy method [22] has been used for analytical continuation of the diagonal part of the Green function matrix to the real energy axis.

Firstly, in Fig.2 we show the total density of states for both conventional single site (DMFT) and the cluster (CDMFT) dynamical mean field theory where only local electron correlations have been included. The QMC simulation has been carried out for $\beta=20$ eV $^{-1}$ which corresponds to a temperature of $T \simeq 580$ K which is on the border of the metal-insulator transition. In the upper panel of Fig. 2 are shown the results of DMFT calculations with $U=2,3,4$ eV and exchange parameter $J=0.5$ eV. For all values of Coulomb interactions there is a peak below the Fermi level at around -0.5 eV, predominantly of a_{1g} character with in all cases the same intensity. Above the Fermi level there are two peaks. The first is at 0.5 eV and has e_g character while the other peak is strongly dependent on the Coulomb parameter and can be associated with an upper Hubbard band. A lower Hubbard band can be seen at around -2 eV. We see that for all values of U the the shape of pseudogap is unchanged and the system remains metallic. On the lower part of Fig. 2 the results of the CDMFT calculation are shown for the same values of the Coulomb and exchange parameters. The general structure of the DOS is seen to be similar to the single site calculation, however one may note interesting differences. The lower a_{1g} quasiparticle band is decreased in intensity and shifted towards the Fermi level from -0.6 eV to -0.3 eV on increasing U from 2 to 4

eV. This has the result that for $U=4$ eV the pseudogap is now located directly at Fermi level, whereas for other U -values and for all DMFT results it lies on the slope of quasiparticle peak.

Using the temperature DOS at the Fermi level, defined as $N(0) \equiv -ImG(\omega_0)/\pi$ with $\omega_0 = \pi T$ we are able to estimate at what values of U the system will become insulating. This is indicated in the inset in the upper panel of the Fig. 2. We see that for the single site calculations $N(0)$ depends weakly on U and the system will remain metallic up to very large values, about 8 eV, of the Coulomb parameter. On the other hand for the cluster calculation $N(0)$ is seen to decrease strongly as a function of U for both values of exchange parameter, and the critical value for an insulating solution is now lower at $U \sim 5-6$ eV. As expected for the d^1 configuration the finite value of the exchange parameter effectively decreases the Coulomb interaction matrix. We see the single site results are in greater contradiction to the experiment as compared to LDA (see Fig. 3): the local Coulomb interaction leads to the reduction of the bonding-antibonding splitting of the a_{1g} subband and this acts to suppress gap formation. On the other hand in the cluster case a small semiconducting gap is developed for large U due to dynamical antiferromagnetic correlation in the Ti-Ti pair.

Nevertheless, using either the DMFT or CDMFT schemes with only local correlations there remains a dramatic absence of gap formation in Ti_2O_3 . We now deploy the full non-local correlation in CDMFT to the effect of non-local correlations on low and high temperature electronic structure. We have used different values of the non-local Coulomb parameters and found that the most important correspond to non-diagonal interactions. For both structures we have chosen values of $U=2$ eV and $J=0.5$ eV which are close to those from constrained LDA estimations [23], while the off diagonal Coulomb parameter W has been chosen at $W=0.5$ eV [24]. On the upper panel of Fig. 3 is shown the total and partial DOS for $\beta=20$ eV $^{-1}$. Shown also is the LDA result. One can see that for the reasonable parameters chosen we can reproduce the correct value of the semiconducting gap ~ 0.1 eV while keeping the bonding-antibonding splitting on the LDA level. In the lower panel the high temperature metallic solution corresponding to $\beta=10$ eV $^{-1}$ is shown. Here we emphasize that the proper inclusion of the structural effect on the LDA level is important as evinced by the fact that for $\beta=20$ eV $^{-1}$ and high temperature hamiltonian we again obtain a metallic solution. The e_g states are similar for both LTS and HTS calculations with a small shift of occupied part in LTS case. However, the difference between the LTS and HTS phases is more pronounced for the a_{1g} states. The bonding-antibonding splitting in the LTS is about 2 eV whereas in the HTS case it is only 1.5 eV. The occupied a_{1g} states in the LTS phase are shifted down opening the insulating gap. The

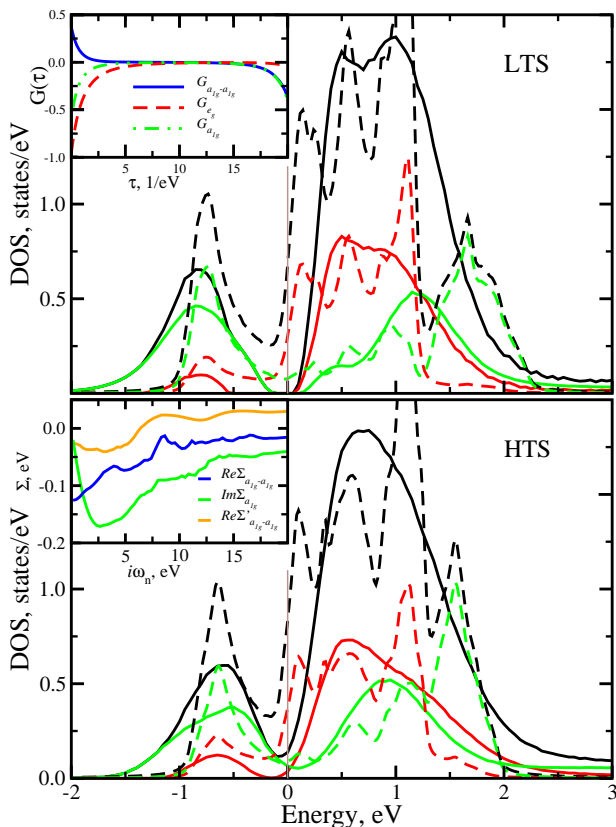


FIG. 3: Partial and total CDMFT (solid line) compared to the LDA (dashed) DOS with $W=0.5$ eV and $V_{a_{1g}}=V_{e_g}=0$. Total DOS are shown by black, the e_g states by red, and a_{1g} states by green. On the upper panel the low temperature structure and $\beta=20$ eV $^{-1}$ are used. For the lower panel the high temperature structure and $\beta=10$ eV $^{-1}$ are used. The diagonal and the biggest a_{1g} off-diagonal Green functions $G(\tau)$ are shown in the upper inset. In the lower inset the $Re\Sigma_{a_{1g},a_{1g}}$ with $W=0.5$ eV are shown by blue, $Re\Sigma'_{a_{1g},a_{1g}}$ with $W=0$ eV by orange and $Im\Sigma_{a_{1g}}$ are shown by green

important difference between the large U and small U plus non-local W is the absence of well defined Hubbard bands. This absence makes possible a critical test of the theory proposed here, and thus it would be very interesting for photo-emission experiments to check the existence or not of a lower Hubbard band at around -2 eV.

We have shown that the cluster LDA+DMFT calculation with a moderate Coulomb repulsion among the a_{1g} orbitals is essential to produce the high temperature semimetallic state and the low temperature insulating state. To understand the role play of the intersite Coulomb interaction we focus on the the quantity $t_{a_{1g},a_{1g}} + Re\Sigma_{a_{1g},a_{1g}}(i\omega)$ which we can interpret as a frequency dependent "effective $a_{1g} - a_{1g}$ hopping" which describes the hopping matrix element in the titanium pair. We find that this quantity is surprisingly frequency dependent (see lower inset of Fig. 3).

We conclude that the main role of the intersite

Coulomb interaction is dynamic (the Hartree contribution to this quantity is small) and results in the effective $a_{1g} - a_{1g}$ hopping that *increases* as the frequency decreases. This enhancement produces a strong level repulsion of the bonding antibonding a_{1g} levels, lowering the a_{1g} level relative to the e_g level at the low frequency. This effect combined with a small narrowing of the a_{1g} band opens the $e_g - a_{1g}$ band gap which results in the insulating state. We checked that this enhancement of the effective hopping as frequency is decreased is absent if we turned off the intersite Coulomb repulsion.

This effect is the cluster DMFT analog of a mechanism first discussed in the context of the single impurity model by Haldane [25]. He observed, that a Coulomb repulsion between the impurity level and additional conduction electron states or screening channels, *enhances* the hybridization (single impurity analog of the hopping matrix element) as we renormalize to low frequency.

We would like to acknowledge O.K. Andersen, V.I. Anisimov, A. Georges and M.I. Katsnelson for useful discussions. This work was supported by the Netherlands Foundation for the Fundamental Study of Matter (FOM). GK was supported by the ONR, grant N000140210766. The authors are grateful to the Kavli Institute of Theoretical Physics, Santa Barbara, for hospitality during the initial stages of this work. This research was supported in part by the National Science Foundation under Grant No. PHY99-07949.

-
- [1] M. Imada, A. Fujimori, Y. Tokura, Rev. Mod. Phys. **70**, 1039 (1998).
 - [2] S.-K. Mo, J.D. Denlinger, H.-D. Kim *et. al.* Phys. Rev. Lett. **90**, 186403 (2003).
 - [3] A. Georges, G. Kotliar, W. Krauth, M. Rozenberg, Rev. Mod. Phys. **68**, 13 (1996).
 - [4] K. Held, G. Keller, V. Eyert, D. Vollhardt, V.I. Anisimov, Phys. Rev. Lett. **86**, 5345 (2001).
 - [5] K.E. Smith and V.E. Henrich, Phys. Rev. B. **38**, 5965 (1988).
 - [6] J. B. Goodenough, Prog. Solid State Chem. **5**, 145 (1972).
 - [7] R.M. Moon, T. Riste, W.C. Koehler, S.C. Abrahams, J. Appl. Phys. **40**, 1445 (1969).
 - [8] S.C. Abrahams, Phys. Rev **130**, 2230 (1963). C.E. Rice, W.R. Robinson, Acta Cryst. B **33**, 1342 (1977).
 - [9] L.F. Mattheiss, J. Phys.: Condens. Matter **8**, 5987 (1996).
 - [10] H. J. Zeiger, Phys. Rev. B. **11**, 5132 (1975).
 - [11] H. Nakatsugawa and E. Iguchi, Phys. Rev. B. **56**, 12931 (1997).
 - [12] M. Catti, G. Sandrone, and R. Dovesi, Phys. Rev. B. **55**, 16122 (1997).
 - [13] R. Shiina, F. Mila, F.-C. Zhang, T. M. Rice, Phys. Rev. B. **63**, 144422 (2001).
 - [14] I.S. Elfimov, T. Saha-Dasgupta, M.A. Korotin, cond-mat/0303404 (2003).
 - [15] A. I. Lichtenstein and M. I. Katsnelson, Phys. Rev. B

- 62**, 9283(R) (2000).
- [16] G. Kotliar, S.Y. Savrasov, G. Palsson, G. Biroli, Phys. Rev. Lett. **87**, 186401 (2001) .
- [17] V.I. Anisimov, A.I. Poteryaev, M.A. Korotin, A.O. Anokhin, G. Kotliar, J. Phys.: Condens. Matter **9**, 7359 (1997). A.I. Lichtenstein and M.I. Katsnelson, Phys. Rev. B **57**, 6884 (1998).
- [18] O.K. Andersen and T. Saha-Dasgupta, Phys. Rev B **62**, 16219 (2000).
- [19] R. Frésard and G. Kotliar, Phys. Rev. B **56**, 12909 (1997).
- [20] J.E. Hirsch and R.M. Fye, Phys. Rev. Lett. **56**, 2521 (1986).
- [21] M.J. Rozenberg, Phys. Rev. B **55**, R4855, (1997).
- [22] M. Jarrell and J.E. Gubernatis, Physics Reports **269**, 133 (1996).
- [23] I. Solov'yev, N. Hamada, K. Terakura, Phys. Rev. B **53**, 7158 (1996).
- [24] G. Lucovsky, R.J. Sladek, J.W. Allen, Phys. Rev. B **16**, 5452 (1977).
- [25] F.D.M. Haldane, Phys. Rev. Lett. **40**, 416 (1978) and Ph. D. Thesis University of Cambridge, 1977. See also Q. Si and G. Kotliar, Phys. Rev. Lett. **70**, 3143 (1993). Q. Si and G. Kotliar, Phys. Rev. B **48**, 13881 (1993).